Non-invasive on-skin sensors for brain machine interfaces with epitaxial graphene

Journal of Neural Engineering

PAPER

Non-invasive on-skin sensors for brain machine interfaces with epitaxial graphene

Shaikh Nayeem Faisal[1], **Mojtaba Amjadipour**[1], **Kimi Izzo**[1], **James Aaron Singer**[1], **Avi Bendavid**[2], **Chin-Teng Lin**[3] and **Francesca Iacopi**[1,4,*]

[1] School of Electrical and Data Engineering, Faculty of Engineering and Information Technology, University of Technology Sydney, Ultimo, NSW, 2007, Australia
[2] CSIRO Manufacturing, 36 Bradfield Road, Lindfield, NSW 2070, Australia
[3] Australian Artificial Intelligence Institute, FEIT, University of Technology Sydney, Ultimo, NSW 2007, Australia
[4] Australian Research Council Centre of Excellence for Transformative Meta-Optical Systems, University of Technology Sydney, Ultimo, NSW 2007, Australia
* Author to whom any correspondence should be addressed.

E-mail: francesca.iacopi@uts.edu.au

Keywords: epitaxial graphene (EG), silicon carbide (SiC), brain–machine interfaces (BMIs), electroencephalogram (EEG)

Supplementary material for this article is available online

OPEN ACCESS

RECEIVED
16 September 2021

REVISED
24 November 2021

ACCEPTED FOR PUBLICATION
6 December 2021

PUBLISHED
23 December 2021

Abstract

Objective. Brain–machine interfaces are key components for the development of hands-free, brain-controlled devices. Electroencephalogram (EEG) electrodes are particularly attractive for harvesting the neural signals in a non-invasive fashion. *Approach.* Here, we explore the use of epitaxial graphene (EG) grown on silicon carbide on silicon for detecting the EEG signals with high sensitivity. *Main results and significance.* This dry and non-invasive approach exhibits a markedly improved skin contact impedance when benchmarked to commercial dry electrodes, as well as superior robustness, allowing prolonged and repeated use also in a highly saline environment. In addition, we report the newly observed phenomenon of surface conditioning of the EG electrodes. The prolonged contact of the EG with the skin electrolytes functionalize the grain boundaries of the graphene, leading to the formation of a thin surface film of water through physisorption and consequently reducing its contact impedance more than three-fold. This effect is primed in highly saline environments, and could be also further tailored as pre-conditioning to enhance the performance and reliability of the EG sensors.

1. Introduction

Brain–machine interfaces aim to be a communicative bridge between the human brain and external electronic systems, integrating seamlessly biological electric pulses (biopotentials) with electronic devices. Non-invasive interfaces can be employed to detect the cortical electrical activity (brain waves) through electroencephalogram (EEG) analysis to interpret human intentions and translate them, for instance, into commands directed to electronic robots [1, 2]. Brain–machine interfaces are gaining substantial impetus from recent advances in brain science [3–5]. EEG sensors are non-invasive in nature, and they can be hence easily employed for any wanted duration without undergoing delicate surgery procedures. However, their signal collection is significantly challenged by the presence of the skull, acting as a physical barrier with additional complexity caused by the presence of hair and variable scalp conditions [3]. EEG sensors can be classified into two types: wet and dry sensors [3, 4]. Semi-dry sensors, typically based on hydrogels, have recently demonstrated encouraging potential as EEG sensors, however, their development is still at an early stage [5–8]. Although wet electrodes typically offer a lower contact impedance with the scalp, they are not desirable for commercial applications due to their cumbersome deployment outside of a clinical environment [4]. On the other hand, dry on-skin electrodes are more versatile and easy to use [8–11]. Dry EEG sensors can be made wearable, reusable, and they can be easily integrated as part of a cap or helmet, opening up a variety of applications outside of clinical settings [9, 10]. The successful implementation of dry electrodes depends on achieving a lower sensor/scalp

impedance, prolonged reliability of the electrodes, while causing minimal skin reaction or discomfort. More conventional dry EEG sensors have a rather uncomfortable bulky form-factor, while still yielding rather high impedance with poor biocompatibility and limited robustness. Recent advances in soft nanomaterials including nanocarbons have been shown as promising alternative towards improved signal collection at the skull [12–26].

Particularly, graphene is an exceptional two-dimensional (2D) material exhibiting superior biosensing capabilities for electrocardiogram (ECG), surface electromyogram (sEMG), and EEG applications [15–25]. Flexible graphene sensors are gaining a lot of interest for applications for continuous health monitoring and neural interfaces [15–22]. The flexible graphene sensors are generally developed from reduced graphene oxide on flexible polymer substrates like nylon, polydimethylsiloxane, or polyimide [16, 17, 25]. Thin-film tattoo sensors made of chemical vapour deposition graphene on a poly (methyl methacrylate) substrate have recently shown encouraging performances towards hands-free control of electronic devices [16, 20, 21]. The advancement of graphene-based flexible sensors is particularly promising on non-hairy areas and in controlled or clinical environments. However, for prolonged applications in a broad range of environments, including all weather conditions, where long-term and repeated usage with high reliability is necessary, electrodes with higher mechanical stability are more appropriate [26, 27].

Few-layers epitaxial graphene (EG) grown on silicon carbide on silicon substrates could become a material of choice for EEG electrodes that can operate with high reliability in external environments. Graphene's excellent conductivity and biocompatibility, highly adherent to a robust mechanical electrode structure would also offer the capability of integration with silicon electronics for further added functionalities [28–34]. Silicon carbide has already gained attention as material for neural interfaces due to its physical robustness, chemical inertness, hemocompatibility and compatibility with neural cells [35]. The EG on SiC can enhance those beneficial properties by combining the advantages of both materials. Using SiC on silicon substrates brings the additional advantage that silicon can be made flexible through thinning it down below 50 μm thickness, which would be impossible using SiC substrates [36].

Here, we report of a novel dry EEG electrode based EG from cubic SiC on silicon for brain–machine interfaces. The graphene electrodes show enhanced electrochemical properties as compared to commercial dry EEG electrodes, particularly an outstanding reliability. In addition, we report a new key phenomenon we refer to as 'surface conditioning'. We observe a dramatic reduction of the contact impedance of the graphene electrodes with the skin over repeated testing, thanks to the formation of surface functional groups promoting graphene wetting and better ion intercalation, all leading to a strongly improved sensor performance.

2. Experimental methods

3C-SiC (cubic silicon carbide) films epitaxially grown on highly doped Si (100) substrates have been purchased from NOVASiC; a chemical and mechanical polishing procedure was performed (StepSiC® by NOVASiC (France)) [37]. The SiC layer thickness is ∼500 nm. A catalytic alloy approach was employed for the growth of EG on SiC on silicon [28, 29]. A cryopump deposition chamber operating with CD Ar^+ ion and 200 mA current was used for sputtering the metallic layers. A sequential deposition of a Ni layer (∼10 nm) followed by a Cu layer (∼20 nm) was used to fabricate EG. Annealing the metal-coated samples at ∼1100 °C for an hour under vacuum condition (∼10^{-5} mbar) leads to breaking the Si–C bonds thanks to the presence of Ni, and release of the carbon atoms which form graphene on the surface. Ni silicides are the by-product of this process, which are later removed together with any metal residues on the surface using chemical wet etching for 9 h (Freckle solution) [28, 29]. EG/SiC/Si coupons of 1 × 1 cm^2 were used for this study. A Zeiss Supra 55VP SEM was employed for surface imaging. Raman spectra were collected with a WiTec Raman microscope using a green laser (532 nm); the Raman spectra reported here is an average of 2500 single spectra collected over a 100 μm^2 area map. X-ray photoelectron spectroscopy (XPS) was carried out with a Specs PHOIBOS 100 Analyzer operated with a Mg Kα x-ray source and 3 mm spot size. The contact angle measurements were performed using a tensiometer (Sigma 701, Biolin Scientific). An electrochemical workstation (CH Instruments, 660 E Model) was used to assess the electrochemical performance of the cells operating in a three-probe configuration (figure S1 (available online at stacks.iop.org/JNE/18/066035/mmedia)). The primary electrochemical properties of the 3CSiC films and the EG grown on silicon carbide films were characterized in a three-electrode cell using a solution of 0.1 M NaCl in water as electrolyte, with respect to Ag/AgCl electrodes. Cyclic voltammograms (CVs) of the electrodes were taken at a potential window of 0.8 V and electrochemical impedance spectroscopy (EIS) measurements were conducted in the 0.01 Hz–1000 kHz frequency range with a signal amplitude of 5 mV.

2.1. On-skin measurements and helmet tests

The on-skin EIS tests were carried out by mounting the EG on silicon coupon of an area of 1 cm × 1 cm. Double sided carbon tape was attached to the back of the highly doped silicon substrate using a pin button for electrical connection. Note that cubic

heteroepitaxials SiC on silicon grows unintentionally n-type doped, and is hence conductive [34]. In addition, when a doped silicon wafer of p-type polarity is used as the substrate for SiC growth, the SiC/silicon interface becomes highly leaky due to a carrier inversion phenomenon [53, 54], causing altogether the graphene to become effectively in electrical contact with its substrate, hence enabling this simple electrical contact approach from the silicon backside. The resistivity of the highly doped p-type silicon substrates were found in the range of 10–20 Ω cm.

In all on-skin measurements, a three-electrode setup was configured using the EG sensor as the working electrode (WE), Ag/AgCl as the reference electrode (RE) and gold as the counter electrode (CE) with a 4 cm distance between the electrodes. All the EIS measurements were taken across a frequency range of 0.1–10 000 Hz at 5 mV. Variations of the electrode/skin contact impedance is common due to factors such as the occurrence of skin flakes, sweat, and changing environmental conditions. Five EG sensors were fabricated, and the sensors have been tested over ten times to investigate reproducibility.

Each sensor was first tested in a three-electrode cell setup. Subsequently, they underwent on-skin EIS measurements on forearms and forehead. Once the skin contact was established, three to four on-skin EIS sequential measurements were taken at 5 min intervals without breaking the skin contact. Each complete measurement took 3–4 min. The average impedance values and their variation were evaluated in the stable value region, reached after three to five repeated measurements (surface conditioning). In addition, in order to explore the robustness of the sensors, we have also performed measurements after 10 min interruption of the skin contact, as well measurements in a saline solution soaked cellulose cloth surface (0.01 M phosphate-buffered saline (PBS)).

We have also used liquid exfoliated graphene (LEG) on SiC as a way to compare the performance of the EG versus that of large-grain (several microns), drop-cast graphene. The large flakes of few-layer graphene were synthesized by liquid exfoliation via sheer mixture following the Coleman *et al* methods [39, 40]. The synthesized graphene showed large few layer graphene flakes (figure S5(a)) and typical low-defect Raman spectrum (figure S5(b)). The low concentrated dispersion of graphene in isopropanol was drop-casted on the highly doped 3C SiC/Si substrate and dried before on-skin measurement.

The helmet setup [38] used for this work contains eight channels connected to eight commercial foam sensors (EEE Holter Technology Co., Ltd, Hsinchu, Taiwan). The two frontal channels, which are in contact with the forehead skin, were replaced by the EG sensors for comparison. The wearable sensors were exclusively tested on the researchers who have co-authored this work, who have all agreed to carry out and consented to publish this research.

3. Results and discussion

A schematic of the EG electrode used for EEG is shown in figure 1(a). A highly doped silicon wafer was employed to provide a suitable electrical connection through the back of the electrodes. The surface of the EG-based EEG electrodes was characterized by SEM–energy dispersive spectroscopy (EDS) mapping for elemental analysis (figures 1(b) and (c)).

The EDS data show the typical elements expected for the EG synthesized on 3C-SiC/Si substrates [28–30]. Details about the graphitic nature and carbon lattice defects of the EG were evaluated by extensive Raman spectroscopy mapping at a wavelength of 532 nm. The Raman spectra show four dominant peaks: the longitudinal optical peak of SiC at ∼970 cm^{-1} and graphene-related peaks of D peak at ∼1340 cm^{-1}, G peak at ∼1580 cm^{-1}, and 2D peak at ∼2680 cm^{-1} (figure 1(d)) [36, 41]. The D peak arises from defects within graphene lattice. The intensity ratio between D and G peaks has been widely used as a measure to compare defect density for graphene-based materials, whereas the intensity ratio between the 2D and the G peaks is an indicator of the graphene thickness [36, 41]. Here, the I_D/I_G and the I_{2D}/I_G averaged intensity ratios indicate the presence of low-defect, and one to two layers graphene, respectively. In particular, the I_D/I_G ratio of 0.2 is an indication of an average graphene grain size of about 90 nm [32, 52].

Na^+ and Cl^- in water solution are known to be major components of human sweat and thus main skin electrolytes [42]. CV was hence used to investigate the electrochemical behavior of EG and SiC on silicon films in 0.1 M aqueous NaCl electrolyte at potential limits of 0.8–0.0 V vs Ag/AgCl electrode in a three-electrode system, at a scan rate of 100 mV s^{-1} (figure 2(a)). From the CV curves it is observed that the EG possesses a substantially enhanced (about 1.8 times) capacitive behavior compared to the SiC film on highly doped silicon (figure 2(a)) [43, 44]. The CV curve of SiC shows redox peaks (oxidation peak at 0.28 V and reduction peak at 0.18 V), possibly due to the presence of metallic impurities. We also observe that the initial CV curve of EG shows a slightly resistive behavior, which is reduced upon repeated cycling (the 100th cycle is shown in figure 2). To quantify and compare the transfer impedance between the electrodes and the electrolyte, we employed the EIS technique.

The EIS curves in the aqueous solution (figures 2(b) and S1) indicate an improved transfer impedance for EG after 100 cycles, as compared both with the initial EG cycle, as well as the reference SiC. The measured charge transfer impedance (R_{ct}) for SiC/Si was ∼160 Ω, whereas the initial R_{ct} of the EG was around 60 Ω, reducing to about 20 Ω after 100 cycles.

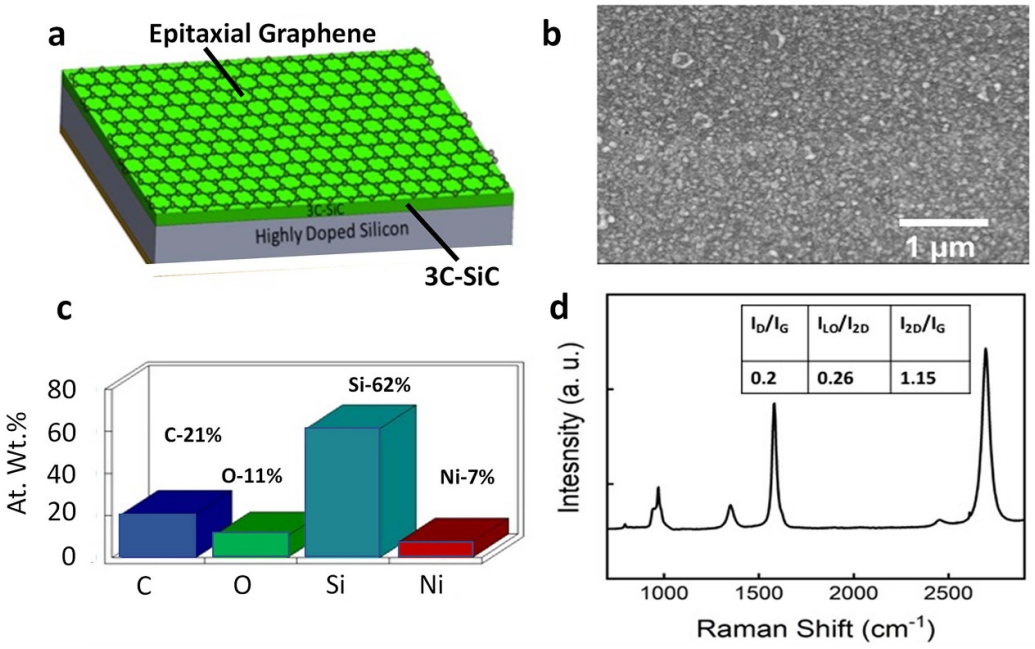

Figure 1. (a) Schematic of the epitaxial graphene electrodes, grown on cubic SiC on highly doped silicon, used as EEG sensors. Characterization of the pristine epitaxial graphene (b) SEM image of the EG surface in pristine condition. (c) Quantitative EDS analysis. (d) Averaged Raman spectrum of the epitaxial graphene collected over a 100 μm^2 area.

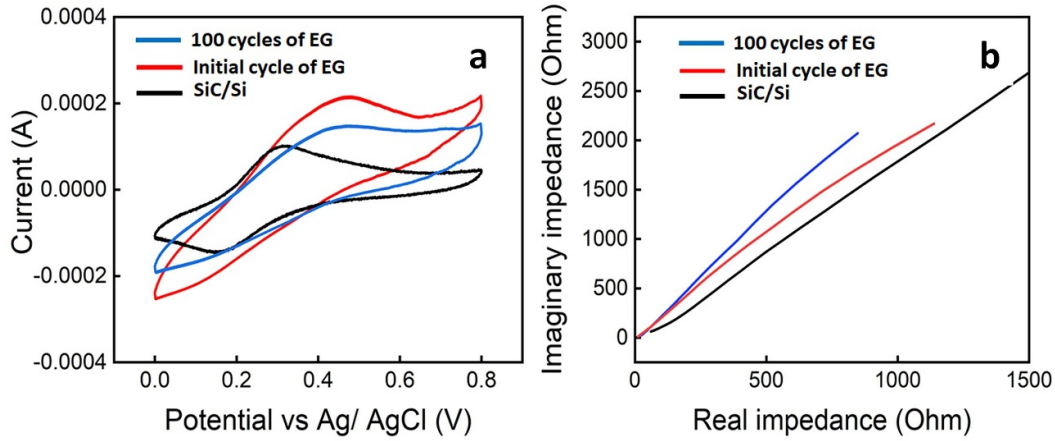

Figure 2. (a) Cyclic voltammograms of EG and SiC on highly doped silicon in 0.1 M NaCl electrolyte at a potential limit of 0.8 V vs Ag/AgCl in a three-electrode system, (b) EIS spectra of the reference bare SiC on silicon film, as well as the first and the 100th cycle of the EG electrode.

3.1. On-skin measurements and surface conditioning

To further evaluate the electrochemical properties of the EG electrode for on-skin applications, the electrode was mounted on a pin button connector using double-sided carbon tape (figure 3(a)). The mounted EG electrode (figure 3(b)) was then placed in contact with the skin surface in a three-electrode configuration as a sensor to measure the impedance spectroscopy. Figure 3(c) represents the circuit diagram of the on-skin EIS measurements and figure 3(d) shows the measurement setup. The WE (green) connected to the EG-based sensors, the CE (red) connected to a gold electrode, and the RE (white) connected to the Ag/AgCl wet electrodes. Gold was chosen as CE type thanks to its highly inert nature.

Figure 4(a) shows the Nyquist impedance plot of the mounted on-skin EG sensor on skin with repeated testing. The skin-contact resistances with impedance reduced drastically after repeated tests and become stable from 3rd test. Figure 4(b) demonstrates the benchmarking of EG sensor to two types of commercial dry EEG sensors measured in exactly the same configuration (conductive foam-based, and spring-loaded gold pin sensors, provided by EEE Holter Technology Co., Ltd, Hsinchu, Taiwan). Note that

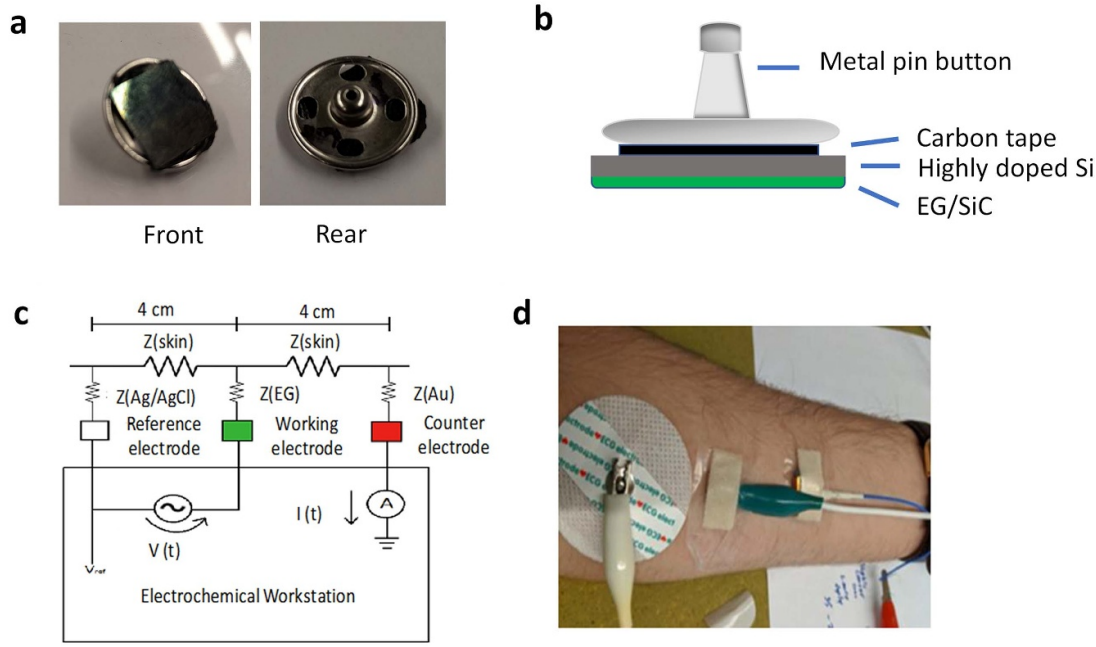

Figure 3. (a) The epitaxial graphene sensors mounted on a metal pin button with carbon tape; (b) schematic showing the approach for the EG electrode mounting for its use as a sensor. (c) Equivalent circuit diagram of the on-skin EIS measurements, and (d) the on-skin EIS setup of the EG sensors on the forearm.

both the foam and EG-based sensors have both the same extent of electrode area exposed to the skin (1×1 cm^2), so they can be directly compared, whereas direct comparisons with the spring-loaded sensor are more difficult because of its pin—contacts and bulky nature (see inset in figure 4(b)).

Results for the first and third repeated (sequential) tests of the EG sensors are also shown, for comparison. While the EG-based sensors do not show an impressive performance at the first test, the impedance resistance reduces drastically after repeated testing. By the third sequential test, the EG sensor reaches an impedance of about 130 kΩ at 50 Hz, making it superior as compared to both the commercial spring-loaded pin sensor (impedance around 830 kΩ at 50 Hz) and commercial conducting foam sensor (impedance around 665 kΩ at 50 Hz). Figure 4(c) shows the sequential evolution of the electrode–skin contact impedance values for the EG sensors at 50 and 100 Hz (average of five measured samples for each point). We can observe that stable impedance values are obtained approximately after two to three sequential tests (figure 4(c)). The measured values of contact impedance once reached stability are found to be 550 ± 10 kΩ at 5 Hz, 435 ± 10 kΩ at 10 Hz, 130 ± 10 kΩ at 50 Hz, and 80 ± 5 kΩ at 100 Hz. The fluctuation of the values of skin contact resistance with dry electrodes are due to the varying skin moisture condition, potential skin abrasions, and the occurrence of flakes from the scalp [27]. Such values compare favorably with the state-of-the-art EEG sensors [45, 46] as well as to previously reported graphene-based EEG sensors, as shown in table S4.

The electrochemical characterization indicates a consistent and marked reduction of contact impedance between the graphene sensors and the skin over repeated sequential testing, until a stable plateau is reached at impedance values that are less than one fourth of the initial ones (figure 4(c)). The repeated tests after keeping the sensor on the air exposure for 10 min showed the similar behavior of reaching the stable values on 2nd test (figure 4(c)).

In addition, a very similar behavior is also observed when the sensors are placed in contact with the aqueous 0.1 M PBS-soaked cellulose cloth in figure 4(d), with a marked reduction in impedance over time. Note that the contact impedance values with the cloth are overall substantially lower than those with the skin, as with average values around ∼6.5 ± 0.5 kΩ at 50 Hz, and ∼4 ± 0.5 kΩ at 100 Hz after reaching stability. This all indicates that the presence of a saline solution at the interface between the graphene electrodes and their contacts (skin or cloth) is very beneficial towards lowering the overall contact impedance.

Hereon, we refer to this phenomenon as 'surface conditioning' of the EG.

3.2. X-ray photoelectron analysis

There is very limited information available to-date regarding a possible on-skin surface conditioning effect of graphene EEG sensors. To this purpose, the EG electrodes have been further characterized to identify any physical and chemical changes after the repeated contact impedance tests in contact with the skin. Optical microscopy and SEM analysis do

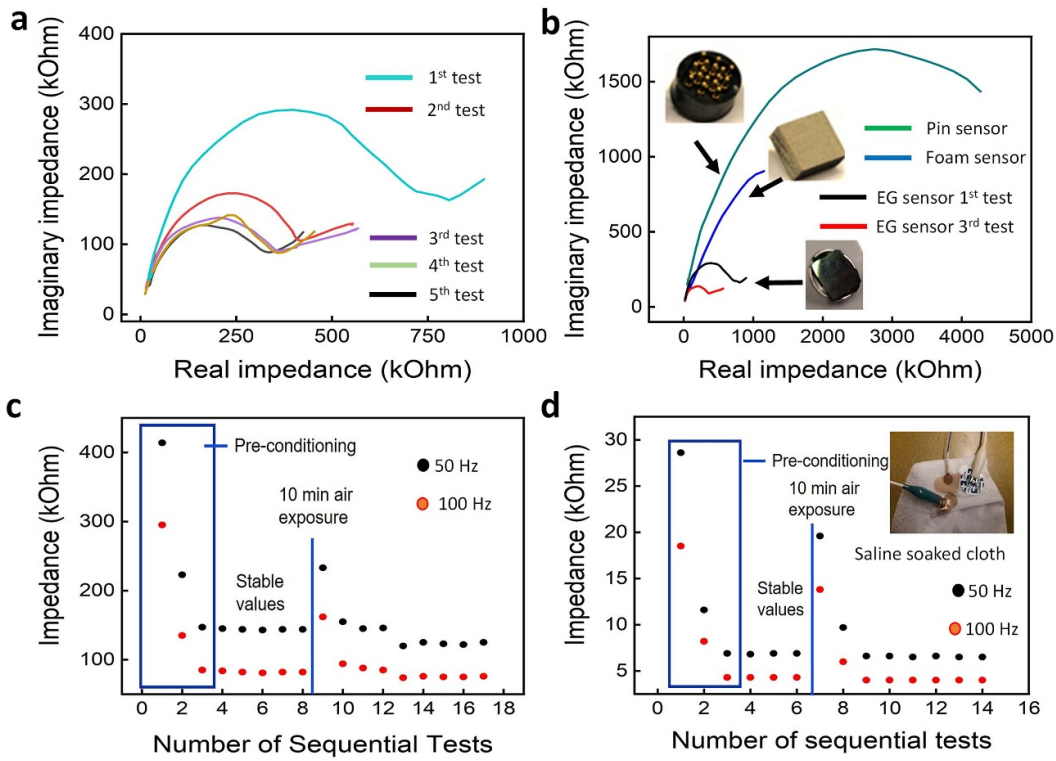

Figure 4. (a) The Nyquist plots of the epitaxial-graphene-based EEG sensors with repeated tests, (b) the Nyquist plot comparison of the epitaxial-graphene-based EEG sensors with foam-based, and spring-loaded ones. The insets show images of the commercial sensors. (c) Magnitude of contact impedance on-skin for the EG-based sensors presented versus the number of sequential tests performed at a frequency of 50 Hz and 100 Hz without breaking the contact with the skin and repeat after 10 min interval of air exposure of the sensor. (d) Magnitude of contact impedance on a saline-soaked cloth for the EG-based sensors presented versus the number of sequential tests performed at a frequency of 50 Hz and 100 Hz without breaking the contact with the skin, and the resumed measurements after 10 min interruption of the sensor contact with the skin (air exposure), (inset) three electrodes EIS measurement setup onto a 0.01 M PBS solution-soaked cloth.

not indicate flagrant changes, except for the presence of skin flakes after the EG has been in contact with the skin (figure S5). However, SEM–EDS mapping after repeated testing revealed a significant increment of surface oxygen (figure S2). This increased oxygen content indicates the possibility of a chemical modification of graphene after contact with the skin, so an XPS analysis was conducted to corroborate this hypothesis.

The XPS surveys comparing the chemical composition of the pristine EG electrode versus that after repeated EIS testing are shown in figures 5(a)–(b) and confirm an increment of surface oxygen after contact with the skin. In particular, the survey analysis, indicates an increase from 15.12 at.% to 21.48 at.% of oxygen, suggesting the likelihood of the formation of new surface oxygen functionalities (table 1). The analysis of the C1s and O1s XPS peaks bring further insights (figures 5(c)–(d) and table 1).

Through the deconvolution of the C1s peak of the pristine EG surface, we find the presence of an estimated 65.1, 25.4, 5.9 and 3.7 at.% of C–C (graphenic), Si–C, C–OH (chemisorbed water) and COOH (carboxyl) bonds, respectively. After repeated testing, a minor decrease of C–C bonds, and high relative decrement of Si–C bonds is observed, while the amount of COOH remains roughly the same, but a significant increment of C–OH occurs. This delivers a strong indication of the formation of surface or edge functionalization with hydroxyl groups on the EG after skin contact. The deconvolution of O1s XPS peaks was also carried out in figures 5(e) and (f). Three types of oxygen bond configurations are inferred: COOH at 531.8 eV, C–OH at 533 eV and chemisorbed water at 534.2 eV. On the pristine graphene, the ratios of the three types of bonds are about 29.8, 15.8 and 54.4 at.% for COOH, C–OH and chemisorbed water, respectively. After repeated testing, the COOH amount remains roughly unvaried, while a strong increment of C–OH (64.5 at.%) and decrement of chemisorbed water (8.3 at.%) were observed.

3.3. Surface conditioning mechanism

Typically, the formation of oxygen functional groups on the graphene surface leads to formation of defects on the basal planes [32]. Therefore, Raman spectroscopy was employed to explore a possible increase in the number of defects created after repeated testing, to reflect the larger amounts of functional groups. However, no significant change is observed in the D peak intensity nor the ratio of I_D/I_G (figure S2(c)).

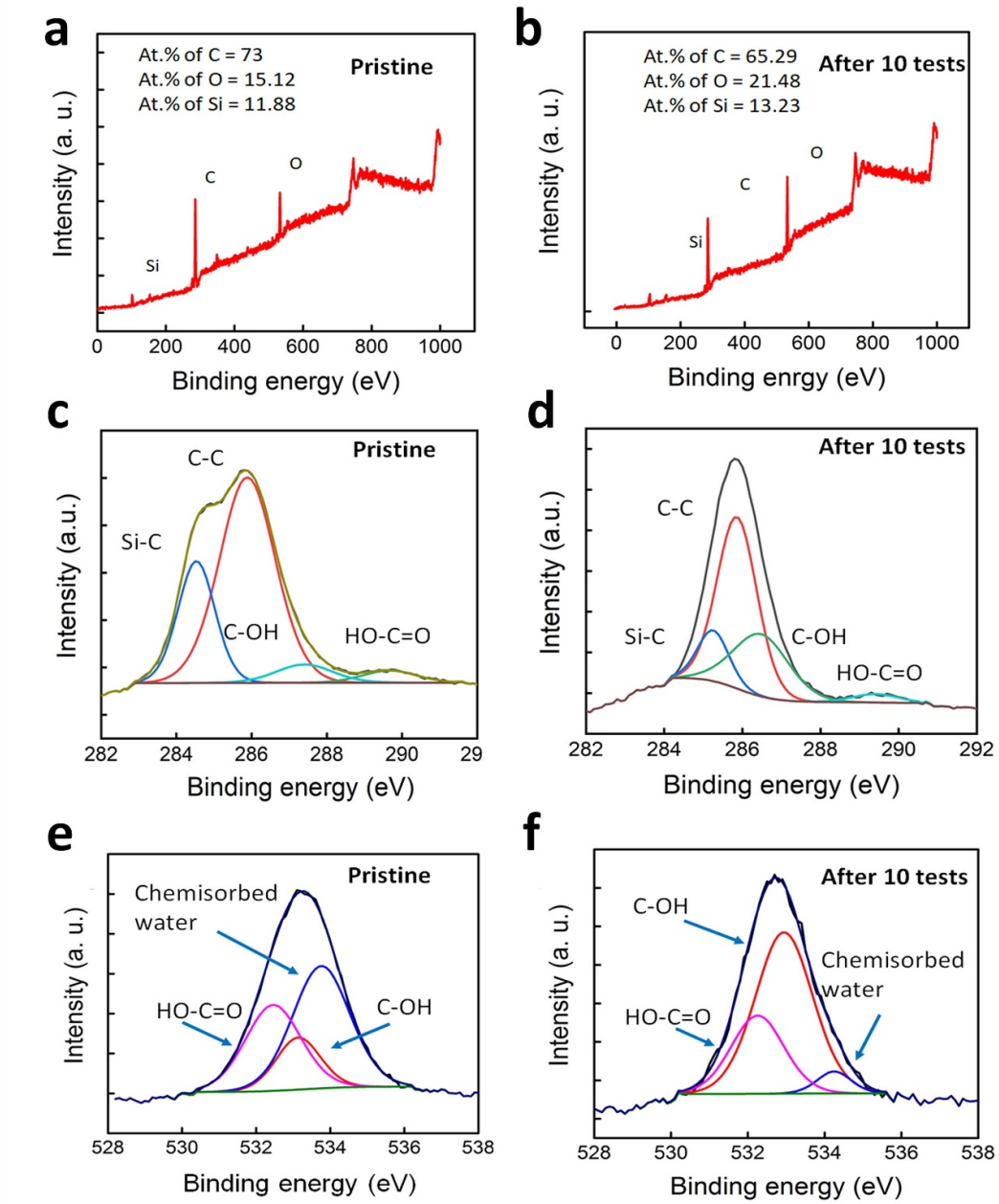

Figure 5. (a) XPS survey analysis of a pristine EG electrode surface, (b) after ten sequential tests, (c) C1S deconvolution of pristine EG and (d) after ten repeated tests, (e) O1s deconvolution of pristine and (f) after ten sequential tests.

Table 1. XPS analysis, including estimated at.% for the different elements from survey spectra, and identified bonds from the deconvolution of the C1s and O1s XPS peaks.

Elements and bond types	Pristine (at.%)	After ten sequential tests (at.%)
C	73	65.29
Si	11.88	13.23
O	15.12	21.48
C1s analysis		
C=C	65.1	55.95
Si–C	25.38	12.98
C–OH	5.85	27.89
COOH	3.71	3.17
O1s analysis		
C–OH	15.8	64.5
COOH	29.8	27.2
Chemisorbed water	54.4	8.3

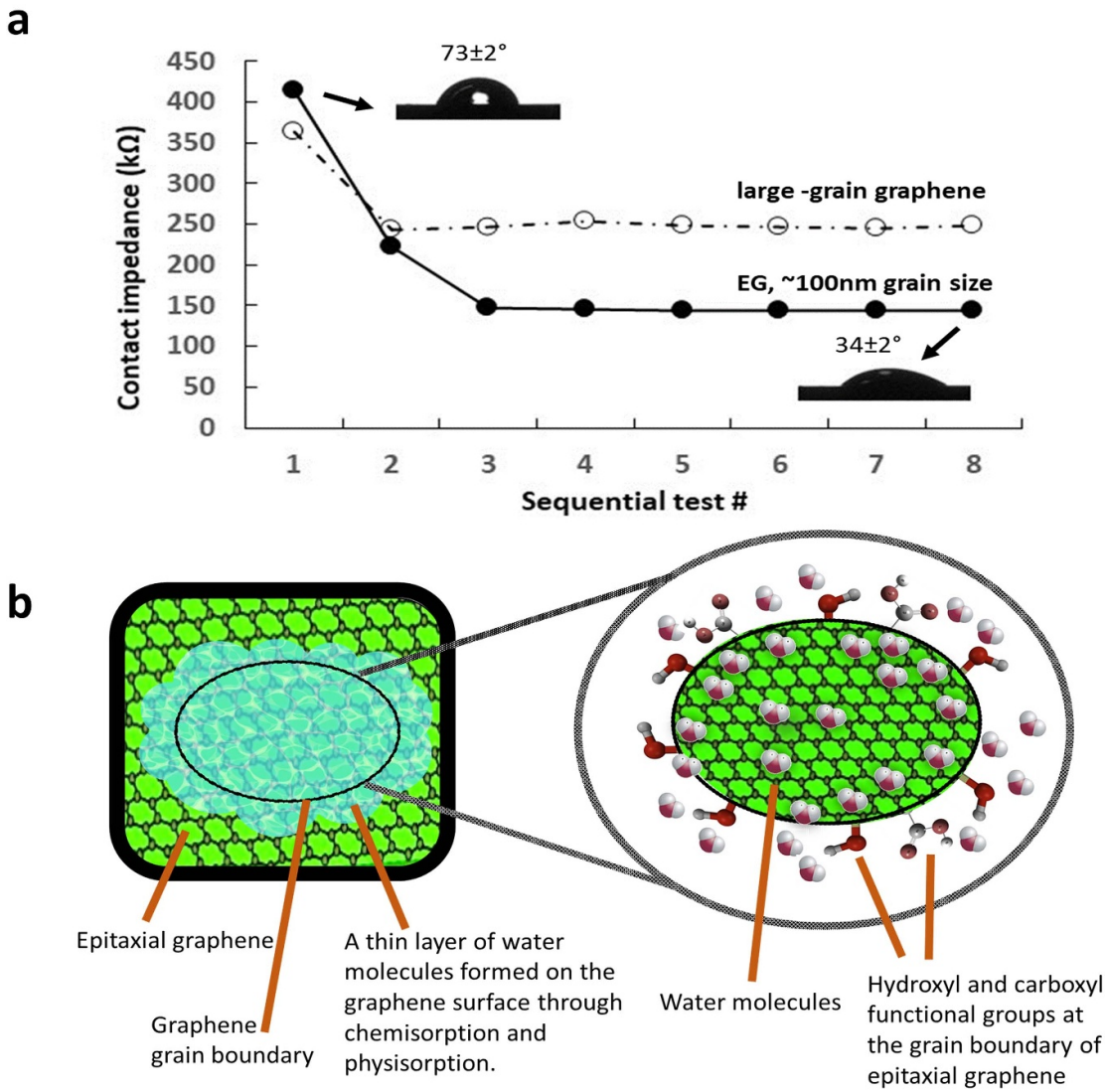

Figure 6. (a) Comparison of the extent of surface conditioning obtained upon sequential on-skin testing of epitaxial graphene sensors with small grain size, versus sensors using liquid exfoliated graphene, with microns grain sizes. The contact angles with water for pristine epitaxial graphene and epitaxial graphene after surface conditioning are shown in the inset images.
(b) Schematic of the chemisorption and physisorption of water on the surface of epitaxial graphene, proceeding through an increased functionalization of the EG grain boundaries with hydroxyl groups after contact with the skin. Over time, a thin layer of water molecules (boundary layer) develops to cover the EG grains, leading to a reduced contact impedance with the skin.

This suggests that the formation of the additional C–OH bond occurs mainly at the edges or grain boundaries of the graphene, rather than the basal plane, due to the higher surface energy of the defective grain boundaries promoting the formation of functional groups [47]. Interestingly, a similar surface functionalization phenomenon was observed in our recent study, where water splitting was purposely induced *in-situ* in a supercapacitor cell with graphene electrodes and acidic electrolyte (sulfuric acid and poly vinyl alcohol) [43]. This functionalization, promoted by the availability of free protons and hydroxyl groups in the electrolyte, led to an increased amount of C–OH and COOH functionalization on the graphene, which in turn, among others, greatly improved the wettability of the electrodes to the electrolyte and led to a marked enhancement of the double-layer capacitance.

Similarly, in this case, the increased hydrophilicity of the graphene leads to a better electrolyte wetting and consequently also an enhanced ion intercalation of the EG, hence a reduced contact impedance with the skin. We propose here a mechanism for the reduction of the contact impedance between the skin and the graphene electrode after prolonged contact.

To confirm the change in hydrophilicity originated by the functionalization, contact angle measurements were carried out on the EG sensor surface before any contact with the skin (pristine) and also after ten sequential tests (conditioning). It was observed that the contact angle went down from $73 \pm 2°$ for the pristine surface to $34 \pm 2°$ after surface conditioning (insets of figure 6(a)).

We suggest that during the graphene-skin measurements and contact, the skin electrolyte (sweat) leads to a chemical functionalization of the grain

boundaries of graphene of oxygen functional groups (hydroxyl and carboxyl) [42]. Sweat is a body fluid emitted by the skin containing mainly ions such as sodium, potassium, calcium, magnesium, chloride and lactate, with a slightly acidic pH [48].

Defect-less graphene is highly hydrophobic and would not be easily wetted by sweat. However, this EG does possesses a relatively large amount of grain boundaries (∼90 nm average grain size), which are chemically active sites. Upon EG-skin contact, hydroxyl groups already present in the sweat solution can form C–OH bonds at the grain boundaries of EG (figure 6). Subsequently, water molecules of sweat can be adsorbed on the surface (physisorption) starting from hydroxyls at the grain boundaries, and extending over time to cover—partly or fully—the grains forming a boundary layer held by weak van der Waals forces on the graphene surface. The decrease of the intensity of C–C and Si–C after repeated testing, is a further indication that a layer is being formed on the top of the graphene upon contact with the skin. This semisolid layer leads overall to an improved wetting of EG and facilitates ion intercalation in the graphene, leading to a substantial reduction of the contact impedance of the sensors with the skin.

To understand the stability of the surface water thin layer formed on the EG, we performed repeated cycles of (a) sequential measurements on-skin, followed by (b) 10 min of contact interruption with the skin /exposure to the environment, and subsequently (c) again sequential measurements on-skin (figure 4(c)). This test indicates the contact impedance increases again after the contact with the skin is interrupted, likely due the evaporation of the water boundary layer. However, the low contact impedance with the skin can be restored again once the contact is re-established. There is also an indication of faster surface re-conditioning, indicating that once the additional C–OH functionalization is in place on the grain boundaries, the formation of the water boundary layer can immediately take place. Recent literature on water adsorption on EG is in line with the proposed mechanism of the formation of water boundary layer [49].

To emphasize the crucial effect of grain boundaries in this mechanism, the extent of surface conditioning upon sequential on-skin testing of the EG sensors was compared to that of sensors using defect-free LEG (figure S5), drop-casted on the silicon carbide on silicon. LEG has micron-sized grains, as compared to the ∼100 nm grain sizes of the EG. The EIS analysis (figure 6(a)) shows a markedly different behavior. While the EG electrodes show a dramatic ∼threefold reduction of contact impedance upon sequential testing, the reduction of contact impedance for LEG electrodes is limited to ∼1.5 (table S7). This analysis proves the importance of the defects/grain boundaries of the graphene in the surface conditioning mechanism. Hence, in order to obtain a maximum benefit in terms of contact impedance with the skin, the use of a graphene with relatively low grain size like the EG here used, is preferred to the use of large grain-size graphene.

In addition, delamination of the graphene from the sensor was observed using the LEG electrode (figure S6). The additional advantage of the EG is its high adhesion to the substrate which prevents delamination [34]. This is further corroborated by the stability of the EG sensors upon long-term on-skin contact as well as the resilience to corrosive saline environments. The long-term contact stability was observed by performing on-skin measurements on the forehead at an interval of 15 min without interrupting the contact with the skin over 2 h. The results showed a very good stability of the impedance values measured at 10 Hz (figure S8(a)). The stability of the EG sensors in harsh corrosive conditions was also confirmed by measuring the sensors after immersion in a solution of concentrated sodium chloride solution (3 M) for up to 120 days (figure S8(b)). The excellent stability is among others attributed to the high adhesion of the EG to its substrate.

Finally, open circuit potential (OCP) and possible potential shifts were also verified. The open circuit potential had been recorded for the graphene sensors (on-skin of the forearm) during 300 s at 0.5 samples s^{-1}, against an Ag/AgCl RE. The corresponding measurements indicate an OCP with the on-skin electrolyte of about 38 ± 6 mV, with negligible potential drift (figure S9). This compares well with current literature using an equal input voltage of 5 mV, for example the OCP (∼58 mV) of Ag/AgCl coated polyurethane based dry electrodes [50].

Within the frequency range investigated in this work (0.1–1000 Hz), we did not observe any obvious DC potential shifts. The DC potential shifts are typically more pronounced, for slow EEG activity at very low frequency (<0.1 Hz) [51].

3.4. EEG helmet-testing

The typical EEG sensors rely on the detection of frequency generated from the brain by placing the electrodes over the head. To observe the performance of the EG sensors for EEG signal collection, initially we have placed the EG sensor on the forehead skin as a WE, together with silver and gold as RE and CE, respectively, all held tightly to the forehead using an elastic head band (inset figure 7(a)). The skin-contact impedance measured on the forehead without the elastic head band showed lower impedance value (90 ± 5 kΩ at 50 Hz, 128 ± 5 at 10 Hz and 145 ± 5 at 5 Hz) compared to the skin-contact impedance measured on the forearm (130 ± 10 kΩ at 50 Hz). With the aid of the elastic band (inset figure 7(a)) we observed further reduction of the skin-contact impedance (44 ± 4 kΩ at 50 Hz, 68 ± 4 kΩ at 10 Hz and 76 ± 4 kΩ at 5 Hz) from the Nyquist

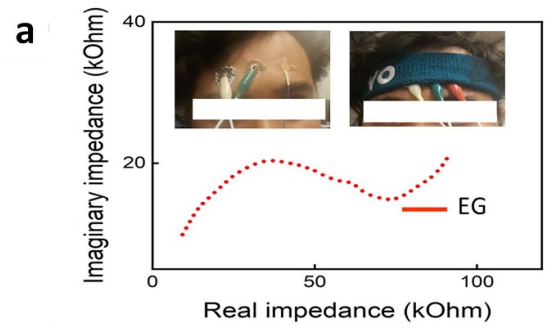

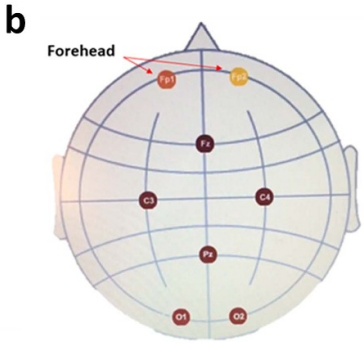

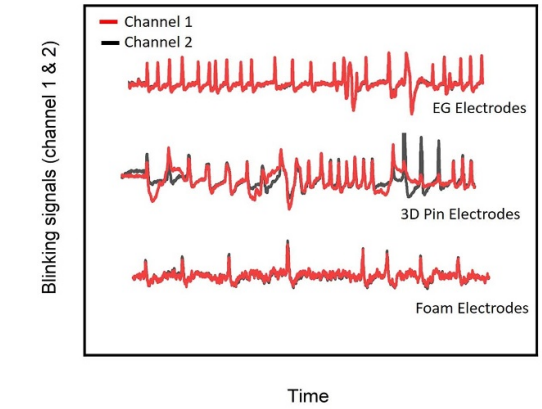

d

EEG Sensors	Channel 1	Channel 2
EG	268 kΩ	238 kΩ
3D Pin	375 kΩ	325 kΩ
Foam	483 kΩ	460 kΩ

Figure 7. (a) Nyquist plot of EIS on the forehead skin using EG sensor as working, Ag/AgCl as reference and gold as counter electrodes by attaching on the skin surface with an elastic head band (inset), (b) a skull map showing the location of the sensors used on the helmet, (c) comparison of signals collected with two channels on forehead using epitaxial graphene (EG), commercial pin and commercial foam sensors, (d) comparison of on-skin impedance values of the sensors mounted the helmet system. Note that a prolonged exposure of the polymer-graphene based electrodes to the skin would typically tend to degrade their performance, for example, because of the graphene's delamination [16]. In this case, exposure to sweat is beneficial as we observed the enhanced conductivity for saline soaked cloth, and we experience no delamination, as the EG displays high adhesion to the underlying SiC layer [34].

plot in figure 7(a). We attribute this improvement to the tighter sensor-skin contact ensured by the elastic band, the harder contact surface offered by the forehead and the sweat generated underneath the band. Finally, the EG-based EEG sensors have been mounted with the help of a simple pin button socket on a brain-interface helmet system (figure 7(b)) [38]. The headset used for collecting the EEG signal has eight channels and the two channels at the forehead, which are in contact with the skin, were replaced by the EG based EEG sensors (figure 7(b)). The graphene-based sensors also show the blinking signal in a similar way to the foam-based sensor (figure 7(c)). This indicates the promising potential of the graphene-based EEG sensors for future brain interface applications.

Figures 7(c) and (d) report a comparison of the signal and impedances from the two forehead channels of the helmet system when EG, commercial foam and commercial pin sensors are used. To evaluate the subject-to-subject variability, the tests of the EG sensors in the helmet system were conducted on a group of eight subjects. From the analysis of the collected data, bearing in mind the variability of skin and hair condition of the different subjects, a reasonable consistency was observed (table S9).

4. Conclusions

In summary, we demonstrated that EG fabricated on silicon carbide on silicon substrates can form robust and reliable electrodes with low contact impedance for brain–machine interface applications. Skin-contact impedance has a crucial effect on the performance of EEG sensors. A repeated sequential testing of the EG sensors leads to a dramatic reduction of over 75% of the contact impedance with the skin. We attribute this improvement to an *in-situ* formation of oxygen functional groups on the graphene grain boundaries upon exposure to the skin, as well as the formation of a thin boundary layer of physisorbed water covering the grains. We refer to this phenomenon as surface conditioning of the EG. This conditioning is consistent and repeatable, and is primed in saline environments. We anticipate that this knowledge may be used to develop a preconditioning procedure to further optimize the EG

EEG sensors' performance. The EG sensors appear hence very competitive with current literature on dry sensors for EEG, EMG and ECG, particularly in terms of resilience, which is crucial to develop real-life reliable on-skin EEG sensor for brain–computer interfaces.

Data availability statement

The data that support the findings of this study are available upon reasonable request from the authors.

Acknowledgments

C T L and F I acknowledge funding from the Defence Innovation Hub, an initiative of the Australian Government, Contract P18-650825. The authors would also like to acknowledge assistance by Mr Daniel Leong, Mr YK Wang and Dr Nguyen Tien Thong Do, Ms Chen Wang and Professor Ho Kyong Shon, as well as the eight volunteers for the EEG tests from our research groups from the Faculty of Engineering and IT, University of Technology Sydney, support by the Australian National Fabrication Facility, node of the University of Technology Sydney.

ORCID iDs

Shaikh Nayeem Faisal https://orcid.org/0000-0003-3317-2282
Mojtaba Amjadipour https://orcid.org/0000-0002-7938-7425
James Aaron Singer https://orcid.org/0000-0003-2226-7753
Avi Bendavid https://orcid.org/0000-0002-2454-9714
Chin-Teng Lin https://orcid.org/0000-0001-8371-8197
Francesca Iacopi https://orcid.org/0000-0002-3196-0990

References

[1] Famm K, Litt B, Tracey K J, Boyden E S and Slaoui M 2013 A jump-start for electroceuticals *Nature* **496** 159–61
[2] Won S M, Song E, Zhao J, Li J, Rivnay J and Rogers J A 2018 Recent advances in materials, devices, and systems for neural interfaces *Adv. Mater.* **30** 1800534
[3] Lin C T, Wu R C, Liang S F, Chao W H, Chen Y J and Jung T P 2005 EEG-based drowsiness estimation for safety driving using independent component analysis *IEEE Trans. Circuits Syst.* I **52** 2726–38
[4] Zhang L *et al* 2020 Fully organic compliant dry electrodes self-adhesive to skin for long-term motion-robust epidermal biopotential monitoring *Nat. Commun.* **11** 4683
[5] Li G, Wang S, Li M and Duan Y Y 2021 Towards real-life EEG applications: novel superporous hydrogel-based semi-dry EEG electrodes enabling automatically 'charge-discharge' electrolyte *J. Neural Eng.* **18** 046016
[6] Li G L, Wu J T, Xia Y H, He Q G and Jin H G 2020 Review of semi-dry electrodes for EEG recording *J. Neural Eng.* **17** 051004
[7] Li G, Wu J, Xia Y, Wu Y, Tian Y, Liu J, Chen D and He Q 2020 Towards emerging EEG applications: a novel printable flexible Ag/AgCl dry electrode array for robust recording of EEG signals at forehead sites *J. Neural Eng.* **17** 026001
[8] Li G, Wang S and Duan Y Y 2018 Towards conductive-gel-free electrodes: understanding the wet electrode, semi-dry electrode and dry electrode-skin interface impedance using electrochemical impedance spectroscopy fitting *Sens. Actuators* B **277** 250
[9] Searle A and Kirkup L A 2000 Direct comparison of wet, dry and insulating bioelectric recording electrodes *Physiol. Meas.* **21** 271–83
[10] Jochumsen M, Knoche H, Kidmose P, Kjaer T W and Dinesen B I 2020 Evaluation of EEG headset mounting for brain-computer interface-based stroke rehabilitation by patients, therapists, and relatives *Front. Hum. Neurosci.* **14** 13
[11] Wu H, Yang G, Zhu K, Liu S, Guo W, Jiang Z and Li Z 2021 Materials, devices, and systems of on-skin electrodes for electrophysiological monitoring and human–machine interfaces *Adv. Sci.* **8** 2001938
[12] Jeong Y C, Lee H E, Shin A, Kim D G, Lee K J and Kim D 2020 Progress in brain-compatible interfaces with soft nanomaterials *Adv. Mater.* **32** 1907522
[13] Araki T, Uemura T, Yoshimoto S, Takemoto A, Nod Y, Izumi S and Sekitani T 2020 Wireless monitoring using a stretchable and transparent sensor sheet containing metal nanowires *Adv. Mater.* **32** 1902684
[14] Fairfield J A 2018 Nanostructured materials for neural electrical interfaces *Adv. Funct. Mater.* **28** 1701145
[15] Ameri S K, Ho R, Jang H, Tao L, Wang Y, Wang L, Schnyer D M, Akinwande D and Lu N 2017 Graphene electronic tattoo sensors *ACS Nano* **11** 7634–41
[16] Das P S, Park S H, Baik K Y, Lee J W and Park J Y 2020 Thermally reduced graphene oxide-nylon membrane based epidermal sensor using vacuum filtration for wearable electrophysiological signals and human motion monitoring *Carbon* **158** 386–93
[17] Li Z, Guo W, Huang Y, Zhu K, Yi H and Wu H 2020 On-skin graphene electrodes for large area electrophysiological monitoring and human-machine interfaces *Carbon* **164** 164–70
[18] Cortadella R G *et al* 2021 Graphene active sensor arrays for long-term and wireless mapping of wide frequency band epicortical brain activity *Nat. Commun.* **12** 211
[19] Qiu J *et al* 2020 A bioinspired, durable, and nondisposable transparent graphene skin electrode for electrophysiological signal detection *ACS Mater. Lett.* **2** 999–1007
[20] Ameri S K, Kim M, Kuang I A, Perera W K, Alshiekh M, Jeong H, Topcu U, Akinwande D and Lu N 2018 Imperceptible electrooculography graphene sensor system for human–robot interface *npj 2D Mater. Appl.* **2** 19
[21] Kireev D, Ameri S K, Nederveld A, Kampfe J, Jang H, Lu N and Akinwande D 2021 Fabrication, characterization and applications of graphene electronic tattoos *Nat. Protocols* **16** 2395–417
[22] Murastaov G *et al* 2020 Flexible and water-stable graphene-based electrodes for long-term use in bioelectronics *Biosens. Bioelectron.* **166** 112426–36
[23] Devi M, Vomero M, Fuhrer E, Castagnola E, Gueli C, Nimbalkar S, Hirabayashi M, Kassegne S, Stieglitz T and Sharma S 2021 Carbon-based neural electrodes: promise and challenges *J. Neural Eng.* **18** 041007
[24] Romero F J, Castillo E, Rivadeneyra A, Lopez A T, Becherer M, Ruiz F G, Rodriguez N and Morales D P 2019 Inexpensive and flexible nanographene-based electrodes for ubiquitous electrocardiogram monitoring *npj Flexible Electron.* **3** 12
[25] Sun B, McCay R N, Goswami S, Xu Y, Zhang C, Ling Y, Lin J and Yan Z 2018 Gas-permeable, multifunctional on-skin electronics based on laser-induced porous graphene and sugar-templated elastomer sponges *Adv. Mater.* **3018** 1804327

[26] Lin S et al 2019 A flexible, robust, and gel-free electroencephalogram electrode for noninvasive brain-computer interfaces *Nano Lett.* **19** 6853–61
[27] Ko L W, Su C H, Liao P L, Liang J T, Tseng Y H and Chen S H 2021 Flexible graphene/GO electrode for gel-free EEG *J. Neural Eng.* **18** 046060
[28] Iacopi F, Mishra N, Cunning B V, Goding D, Dimitrijev S, Brock R, Dauskardt R H, Wood B and Boeckl J 2015 A catalytic alloy approach for graphene on epitaxial SiC on silicon wafers *J. Mater. Res.* **30** 609–15
[29] Mishra N, Boeckl J J, Tadich A, Jones R T, Pigram P J, Edmonds M, Fuhrer M S, Nichols B M and Iacopi F 2017 Solid source growth of graphene with Ni–Cu catalysts: towards high quality *in situ* graphene on silicon *J. Phys. D: Appl. Phys.* **50** 095302
[30] Cunning B V, Ahmed M, Mishra N, Kermany A R, Wood B and Iacopi F 2014 Graphitized silicon carbide microbeams: wafer-level, self-aligned graphene on silicon wafers *Nanotechnology* **25** 325301
[31] Mishra N, Boeckl J, Motta N and Iacopi F 2016 Graphene growth on silicon carbide: a review *Phys. Status Solidi* a **213** 2277–89
[32] Pradeepkumar A *et al* 2020 P-type epitaxial graphene on cubic silicon carbide on silicon for integrated silicon technologies *ACS Appl. Nano Mater.* **3** 830–41
[33] Ahmed M, Wang B, Gupta B, Boeckl J J, Motta N and Iacopi F 2017 On-silicon supercapacitors with enhanced storage performance *J. Electrochem. Soc.* **164** A638
[34] Mishra N, Jiao S, Mondal A, Khan Z, Boeckl J J, Gaskill K D, Brock R E, Dauskardt R H and Iacopi F 2018 A graphene platform on silicon for the internet of everything *IEEE 2nd Electron Devices Technology and Manufacturing Conf. (EDTM)* vol **2018** pp 211–3
[35] Bernardin K, Frewin C L, Everly R, Hassan J U and Saddow S E 2018 Demonstration of a robust all-silicon-carbide intracortical neural interface *Micromachines* **9** 412–30
[36] Schuster C S, Smith B R, Sanderson B J, Mullins J T, Atkins J, Joshi P, McNamara L, Krauss T F and Jenkins D G 2017 Flexible silicon-based alpha-particle detector *Appl. Phys. Lett.* **111** 073505
[37] Portail M, Zielinski M, Chassagne T, Roy S and Nemoz M 2009 Comparative study of the role of the nucleation stage on the final crystalline quality of (111) and (100) silicon carbide films deposited on silicon substrates *J. Appl. Phys.* **105** 083505
[38] Lin C T, King J T, John A R, Huang K C, Cao Z and Wang Y K 2021 The impact of vigorous cycling exercise on visual attention: a study with the BR8 wireless dry EEG system *Front. Neurosci.* **15** 621365
[39] Paton K R *et al* 2014 Scalable production of large quantities of defect-free few-layer graphene by shear exfoliation in liquids *Nat. Mater.* **13** 624–30
[40] Roy A K, Faisal S N, Spickenheuer A, Scheffler C, Wang J, Harris A T, Minett A I and Islam M S 2021 Loading dependency of 2D MoS_2 nanosheets in the capacitance of 3D hybrid microfibre-based energy storage devices *Carbon Trends* **5** 100097
[41] Malard L, Pimenta M, Dresselhaus G and Dresselhaus M 2009 Raman spectroscopy in graphene *Phys. Rep.* **473** 51–87
[42] Chen Y L, Kuan W H and Liu C L 2020 Comparative study of the composition of sweat from eccrine and apocrine sweat glands during exercise and in heat *Int. J Environ. Res. Public Health* **17** 3377
[43] Amjadpour M, Su D and Iacopi F 2020 Graphitic-based solid-state supercapacitors: enabling redox reaction by *in situ* electrochemical treatment *Batter. Supercaps* **3** 587–95
[44] Faisal S N *et al* 2018 Nanoarchitectured nitrogen-doped graphene/carbon nanotube as high performance electrodes for solid state supercapacitors, capacitive deionization, Li-ion battery, and metal-free bifunctional electrocatalysis *ACS Appl. Energy Mater.* **1** 5211–23
[45] Fu Y, Zhao J, Dong Y and Wang X 2020 Dry electrodes for human bioelectrical signal monitoring *Sensors* **20** 3651
[46] Al-Qazzaz N K, Ali S H B M, Ahmed S A, Chellappan K, Islam M S and Escudero J 2014 Role of EEG as biomarker in the early detection and classification of dementia *Sci. World J.* **2014** 906038
[47] Yu W, Sisi L, Haiyan Y and Jie L 2020 Progress in the functional modification of graphene/graphene oxide: a review *RSC Adv.* **10** 15328–45
[48] Sato K, Wang W H, Saga K and Sato K T 1989 Biology of sweat glands and their disorders. I. Normal sweat gland function *J. Am. Acad. Dermatol.* **20** 537–63
[49] Burghaus U 2021 Adsorption of water on epitaxial graphene *J. Mater. Res.* **36** 129–39
[50] Vasconcelos B, Fiedler P, Machts R, Haueisen J and Fonseca C 2021 The arch electrode: a novel dry electrode concept for improved wearing comfort *Front. Neurosci.* **15** 748100
[51] Voipio J, Tallgren P, Heinonen E, Vanhatalo S and Kalia K 2003 Millivolt-scale DC shifts in the human scalp EEG: evidence for nonneuronal generator *J. Neuropysiol.* **89** 2208–14
[52] Ferrari A C 2007 Raman spectroscopy of graphene and graphite: disorder, electron–phonon coupling, doping and nonadiabatic effects *Solid State Commun.* **143** 47–57
[53] Zielinski M, Portail M, Roy S, Chassagne T, Moisson C, Kret S and Cordier Y 2009 Elaboration of (111) oriented 3C-SiC/Si layers for template application in nitride epitaxy *Mater. Sci. Eng.* B **165** 9–14
[54] Pradeepkumar A, Zielinski M, Bosi M, Verzellesi G, Gaskill D K and Iacopi F 2018 Electrical leakage phenomenon in heteroepitaxial cubic silicon carbide on silicon *J. Appl. Phys.* **123** 215103